FULL PAPER

Surface Modified Low Cost Adsorbent in Malachite Green Scavenging, Malachite Green/Rhodamine B and Malachite Green/Rhodamine B/Cu²⁺ Composite Treatment

Adejumoke A. Inyinbor[a*], Oluwasogo A. Dada[a], Olugbenga S. Bello[b], Abimbola P. Oluyori[a], Oluwapamilerin F. Fanawopo[a], Toyin A. Oreofe[c], and Oluwafunmilayo Ajayi[d]

[a]Department of Physical Sciences, College of Pure and Applied Sciences, Landmark University, P.M.B 1001, Omu Aran, Nigeria.
[b]Department of Pure and Applied Chemistry, Faculty of Sciences, Ladoke Akintola University of Technology, P.M.B. 4000, Ogbomoso, Nigeria.
[c]Department of Chemical Engineering, College of Engineering, Landmark University, P.M.B 1001, Omu Aran, Nigeria.
[d]Department of Chemistry, Faculty of Sciences, Crown Hill University, Eiyenkorin, Ilorin, Nigeria.

Abstract:

Modified Irvingia gabonensis nut waste (MIg) was used for malachite green (MG) removal from aqueous solution. Adsorption operational parameters such as pH, adsorbent load, concentration with contact time were investigated to establish the behavior of MIg for subsequent applications in a complex media. The potency of MIg in the effective treatment of binary and ternary mixture of MG/rhodamine B (RhB) dyes and MG/RhB/Cu²⁺ solution was also studied. Optimum MG adsorption was obtained at pH of 6.0. MG-MIg kinetics adsorption data was best described by the Pseudo second order kinetic model. MG adsorption onto MIg was predominantly onto a uniform site and the maximum monolayer adsorption capacity was obtained to be 250mg/g. MG and RhB synergistically aided the removal of each other both in binary and ternary solutions hence 99.99% removal was observed for the two dyes after treatment with MIg. Cu²⁺ showed no change in concentration after treatment with MIg.

Keywords: adsorption; malachite green; binary; kinetics; isotherms

1. Introduction

Dye utilizing industries use a huge volume of water in their dyeing stage hence large volume of wastewater is generated [1]. Dye wastewater is usually a composite of pollutants and the visible colouration is a firsthand challenge. The failure of the dye processes and techniques releases about half of utilized dye into the environment [2]. The impact of dye wastewater on the water environment range from dissolved oxygen displacement, resistance in sunlight penetration hence various effects on aquatic organisms and plants [3]. For instance, Malachite green is known to be carcinogenic, mutagenic, affects human immune as well as affects human reproductive systems [4]. Heavy metals which forms a composite of dye wastewater are also known carcinogens and mutagens. Effective treatment of dye wastewater is therefore important in order to ensure environmental sustainability.

Precipitation, ion exchange, electrochemical treatment, reverse osmosis, membrane filtration and adsorption amongst others have been used for dye and heavy metals removal [5]. Adsorption techniques is a preferred choice due to its

simplicity of operation and the ability to remove very low concentration of pollutants [6, 7]. The cost of activated carbon in use for adsorption techniques makes it less attractive particularly within the nations with growing economy. Hence, the continuous search for suitable, efficient and economical substitute. Agrowastes [8], industrial wastes [9], naturally occurring substances such as various types of clay [10-12], silica and fly ash [13, 14], dolomites [15] amongst others have been used for adsorption of various pollutants.

Since dye-laden industrial effluent is usually a composite of dye(s), heavy metal(s), salts, starch amidst others, only multifunctional adsorbent will be suitable for effective treatment of such effluent. While few reports exists on adsorption of dye from their binary and ternary mixtures [16] as well as adsorption of heavy metal from their binary and ternary mixtures [17], to the best of our knowledge, reports focusing on dyes/heavy metal ternary system is scarce. Hence, the importance of this study. A multifunctional adsorbent will go a long way to address the huge environmental challenge posed by the discharge of dye-laden wastewater.

In this study, the efficacy of modified *Irvingia gabonensis* (MIg) in the uptake of Malachite Green (MG). In order to establish the optimum conditions, various adsorption operational parameters were investigated. In addition, MIg multi-adsorption efficacy in composite mixture of rhodamine B (RhB)/MG binary mixture and RhB/MG/aqueous copper (II) ternary solution were also investigated and results herein presented.

2. Results and Discussion

The adsorbate aqueous chemistry and adsorbent uptake ability greatly depends on solution pH. Percentage MG removal rose rapidly from 94.44 to 98.07 % as adsorbate solution pH increased from 2 to 3 (Figure 1). Subsequent percentage removal was minimal until pH of 6 after which negligible percentage MG removal were negligible. The adsorbent pHpzc was earlier reported to be 6.60 [18] hence at low pH, great repulsion occurred between the positively charged adsorbent surface and cationic dye (MG). Adsorbent surface gradually deprotonate as the solution pH rose hence percentage removal also

increased. Hemicellulose based adsorbent used in MG adsorption was reported to have behaved in similar manner [19].
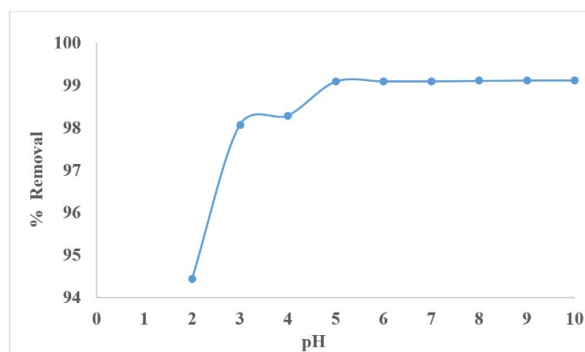
Figure 1. Effects of pH on MG uptake onto MIg [Temperature (26 °C), Adsorbent load (0.1 g) and agitation speed (130 rpm)] [n = 3, 0 ≤ SD ≥ 0.0025].

Adsorbent load effect

MG removal capacity of MIg did not change significantly by increasing adsorbent dosage (Figure 2). Percentage removal was almost at maximum at the minimum dosage hence additional adsorption adsorption sites may overlap.
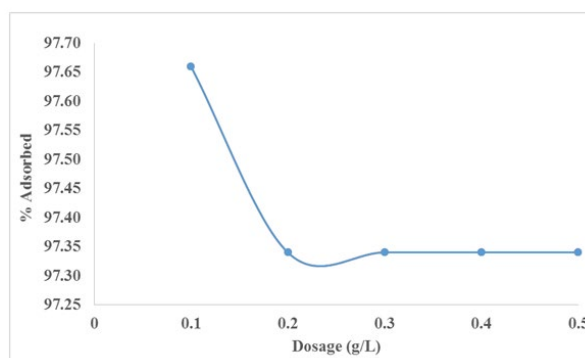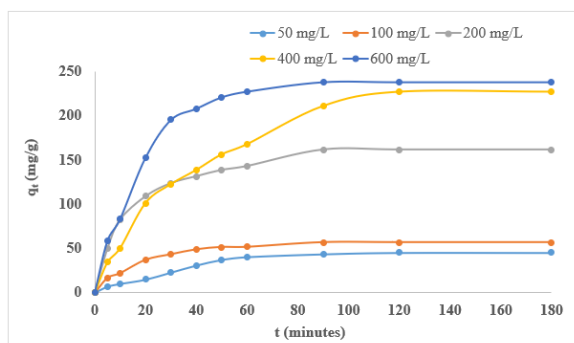

Figure 2. Adsorbent load effect on MG uptake onto MIg [Temperature (26 °C), pH (6.0) and agitation speed (130 rpm)] [n = 3, 0 ≤ SD ≥ 0.0027].

Effect of concentration and contact time

Rapid uptake of MG onto MIg was observed. Within the first 60 minutes quantity adsorbed increased for all concentrations considered (Figure 3). Subsequently, no significant increase in quantity MG adsorption was observed. High concentration provided enough driving force for MG molecules to overcome the mass transfer

88

Orbital: Electron. J. Chem. 12 (2): 87-94, 2020

barrier between the solid-liquid interface. Quantity adsorbed at equilibrium was 238.25 mg/g for the highest concentration studied, this represents 39.71 % of the initial MG in solution. However, for the lowest concentration studied, about 90 % removal was recorded. Quantity adsorbed was obtained to be 45.35 mg/g at equilibrium. The ratio of available adsorption sites to MG concentration was considerable low for the later hence the high removal percentage obtained

Figure 3. Concentration with contact time effects on MG uptake onto MIg [Temperature (26 ^oC), Adsorbent load (0.1 g) and agitation speed (130 rpm)]
[n = 3, 0 ≤ SD ≥ 0.085]

Table 2. Isothermal parameters for the MG-MIg adsorption system.

Isotherms	Constants	MIg
Langmuir	q_{max}(mg/g)	250
	K_L(L.mg^1)	0.048
	R_L	0.0253
	R^2	1.0000
Freundlich	K_F	0.00257
	n	0.5107
	R^2	0.9640
Temkin	A	5.1×10^{77}
	B	0.0101
	b(kJ/mol)	245.304
	R^2	0.8191

Adsorption Isothermal Studies

Relating the amount of MG adsorbed per gram of adsorbent with unadsorbed MG concentration necessitate adsorption isothermal studies. The Langmuir adsorption isotherm which explain the uni-layer adsorption coverage, the Freundlich which describes multi-site adsorption of MG and Temkin adsorption isotherm were used in this study. The adsorption data best fits into the

Langmuir isotherm with correlation coefficient (R^2) of unity (Table 2). The isotherm data constants suggest that adsorption onto a uniform site dominate MIg-MG system, however, some level of multilayer adsorption and adsorbate-adsorbate MG uptake also occurred. Adsorption isotherms order was Langmuir > Fruendlich > Temkin. The maximum monolayer adsorption capacity for the MIg-MG system was obtained to be 250 mg/g, this is observed to present high efficacy than others previously reported in literatures (Table 3).

Table 3. MIg-MG adsorption system maximum monolayer adsorption capacity in comparison with previous literature works.

Adsorbents	q_{max} (mg/g)	Ref
Maize stalk	11.77	[20]
Baggase	46.56	[20]
Maize stalk/nanomaterial	19.46	[20]
Baggase/nanomaterial	60.95	[20]
Almond gum	172.41	[21]
Wood apple shell	80.65	[22]
Treated eucalyptus leave	28.64	[23]
Peltophorum pteocarpum fruit shell	40.00	[24]
Modified Peltophorum pteocarpum fruit shell	62.5	[24]
Magnetic modified activated carbon	217.68	[25]
Raw tarap leave	254.9	[26]
Modified tarap leave	422.00	[26]
Luffa aegyptica peel	70.21	[27]
Modified Luffa aegyptica peel	78.79	[27]
Acid treated coffee husk	195.35	[28]
Modified *Irvingia gabonensis*	250.00	This study

Kinetics studies

The kinetics data are shown in table 4. Judging from the correlation coefficient, the q_{cal} and values obtained for chi square calculations, the pseudo second order kinetics best described the MG-MIg adsorption kinetic data. Several factor is responsible for adsorption rate viz solute diffusion to the film surrounding the particle, particle surface adsorption, adsorbate pore penetration or pore diffusion and various uptake techniques which via mechanisms such as ion- exchange, physicochemical adsorption, complexation or precipitation [28]. However, mechanism of

89

Orbital: Electron. J. Chem. 12 (2): 87-94, 2020

adsorption is better explained via the intraparticle diffusion model of the Weber and Morris. The linearity of the plot of q_t versus $t^{1/2}$ (Figure not shown), since each straight lines did not go through the origin, the intraparticle diffusion is not the only rate determining step. The diffusion rate was observed to increase with concentration up to 400 mg/L suggesting increased drive force due to abundant solute in solution [29]. The increase in boundary layer thickness with increase in concentration suggests higher adsorption capacity at higher concentration.

Table 4. Kinetic model parameters for the adsorption of MG unto MIg.

| Constants	Initial concentration				
	MIg				
	50	100	200	400	600
$q_{e\ experimental}$ (mg/g)	45.9958	56.89214	161.6276	226.763	238.2492
Pseudo first order					
$q_{e\ calculated}$ (mg/L)	39.44	46.95	109.91	239.55	239.36
K_1 (min^{-1})	0.023	0.041	0.031	0.027	0.053
R^2	0.9960	0.9730	0.9730	0.9620	0.9950
χ^2	1.089	2.105	24.335	0.683	0.005
Pseudo second order					
$q_{e\ calculated}$ (mg/g)	53.763	62.111	175.438	285.714	263.157
K_2 X 10^{-4} (gmg^{-1}min^{-1})	6.320	0.125	4.760	8.850	2.830
R^2	0.9997	0.9972	0.9986	0.9903	0.9935
χ^2	1.122	0.439	1.087	12.163	2.357
Intra particle diffusion					
C X 10^2 (mgg^{-1})	5.721	18.661	59.692	11.487	73.815
K_{diff} (mgg^{-1}min$^{-1/2}$)	3.476	3.634	9.473	18.777	15.978
R^2	0.9059	0.76654	0.8067	0.9263	0.7108

Efficacy of MIg in RhB/MG and RhB/MG/Cu^{2+} mixture treatment

Figure 4 shows the RhB/MG and RhB/MG/Cu^{2+} mixtures before and after treatment with MIg. RhB is a xanthene dye with intense colour hence the strong band at 554 nm (λ_{max} of RhB). RhB strength of strong colour gave it wide variation of usage [30, 31]. In the ternary solution, the presence of metal ion further reduced the intensity of MG. RhB and MG removal were aided by the presence of other ions hence almost 100 % removal of RhB and MG was obtained in binary and ternary solution. The initial concentration of Cu^{2+} introduced into the ternary mixture reduced drastically before treatment with MIg. Possible complexation between metal and dye may be responsible for such drastic Cu^{2+} reduction before treatment. High loads of heavy metals in dye wastewater is traced to the use of metal complex dyes [3]. The uncomplexed metal ion left in the ternary solution was not affected by MIg treatment hence Cu^{2+} concentration remain unchanged after MIg treatment (Figure 5).
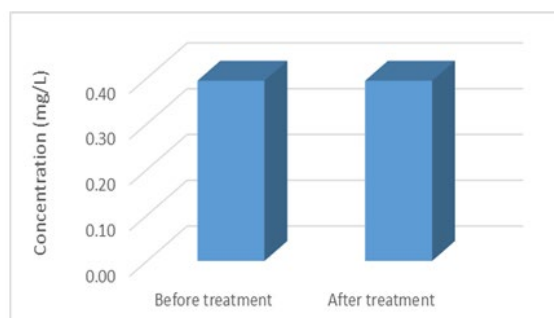
Figure 5. Cu^{2+} concentration before and after MIg treatment.

90

Orbital: Electron. J. Chem. 12 (2): 87-94, 2020
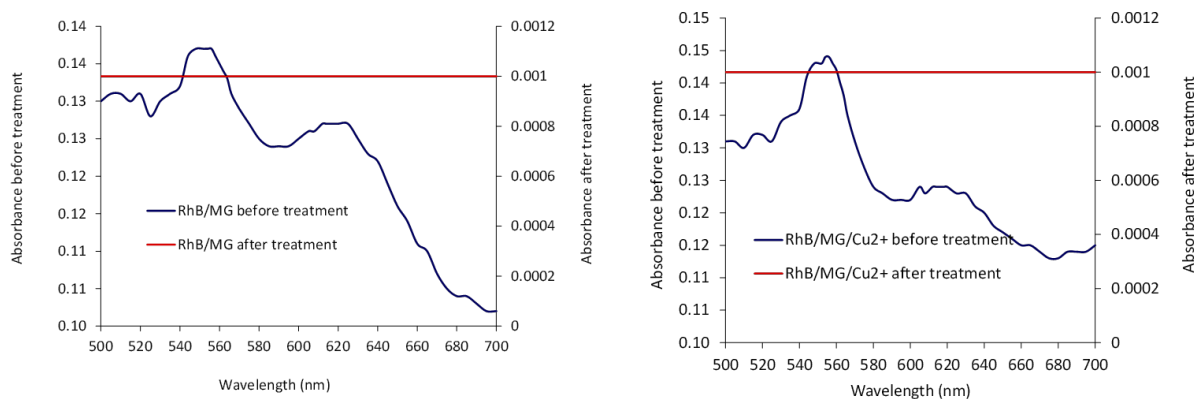
Figure 4. UV/Vis spectral of RhB/MG and RhB/MG/Cu^{2+} before and after treatment with MIg.
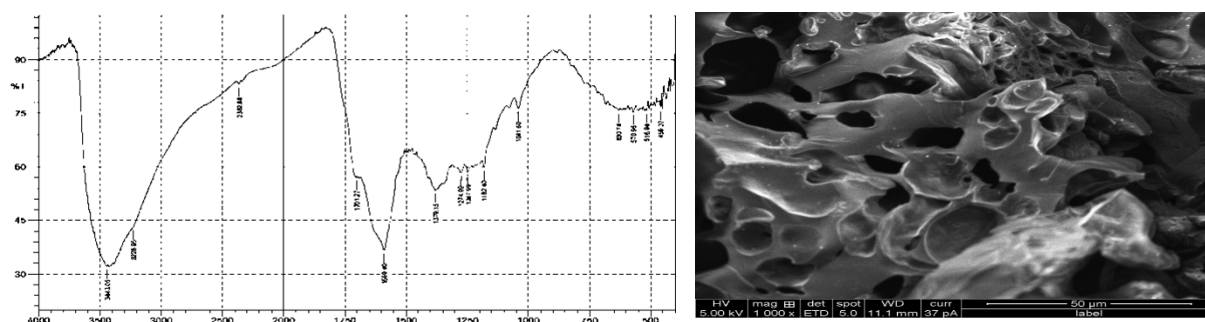
Cost analysis

MIg is a waste which is readily available and at no cost. However, the cost of collection and processing would amount to 0.030 USD/kg (30 USD/ton). MIg is found highly cost effective when compared commercial activated carbon. Hence MIg gives a good economic advantage over commercial activated carbon which is in use conventional adsorption technique.

MIg surface chemistry and surface

morphology

The surface chemistry of MIg as shown from Fourier Transform Infrared Spectroscopy (FTIR) spectrum (Figure 6a). Various absorption peaks such as –OH stretching vibration at 3443 cm^{-1}, the C-OH stretching vibration occurring at 1379 cm^{-1} and the C=C vibration of aromatic observed at 1588 cm^{-1} amongst others are suitable absorption sites. MIg is also characterized with moderately large pores (mesopores) (Figure 6b) known suitable for the uptake of large molecules such as dye [32].

Figure 6. FTIR spectrum of MIg (a), SEM image of MIg (b).

3. Material and Methods

Adsorbent preparation

Collection, pretreatment and modification of *Irvingia gabonensis* waste is as mentioned in our previous work [18]. In brief, biomass was impregnated with concentrated sulphuric acid, followed by a forceful fiber opening via moderate thermal treatment. Modified *Irvingia gabonensis* (MIg) was stored for further use.

Malachite green batch adsorption studies

Stock solution of 1000 mg/L of Malachite Green (MG) was prepared and subsequent lower concentrations used in this study were prepared by serial dilution. Adsorbate existence in solution viz-a-viz adsorbent surface charge and removal characteristics depend greatly on solution pH. Other parameters such as adsorbate concentration, contact time and adsorbent dosage/load contributes to adsorption efficiency of adsorbents. First, studies using 0.1 g adsorbent

91

Orbital: Electron. J. Chem. 12 (2): 87-94, 2020

dispersed in a 100 cm³ of a 50 mg/L MG solution with varied adsorbate solution pH of between 2 and 10 in separate Erlemenyer flask was agitated on a shaker until equilibrium. Afterwards, 100 cm³ of MG solution of varying concentration 50, 100, 200, 400 and 600 mg/L whose pH were adjusted to 6 had 0.1 g adsorbent dosage dispersed in them in separate Erlemenyer flask and were agitated on a shaker until equilibrium was attained. Varying dosage study used 0.1 to 0.5 g adsorbent load while 100 cm³ of 50 mg/L MG solution at pH of 6 were the conditions. Unadsorbed MG and MIg were separated by centrifuge and the concentration of dye left in solution were obtained using a Beckman Coulter Du 730 UV-Visible spectrometer at fixed wavelength of 618 nm. Percentage MG and quantity MG adsorbed at time t were calculated according to equations 1 and 2.

$$\% \, Removal = \frac{(C_i - C_t)}{C_t} \times 100 \qquad \mathbf{1}$$

$$q_t = \frac{(C_i - C_t)}{M} \times V \qquad \mathbf{2}$$

Equations 1 and 2 factors in initial MG concentration (C_i), final MG concentration (C_f), concentration of MG at time t, volume of aqueous MG used in adsorption studies in liters and mass of MIg in grams.

Mathematical modeling of MG-MIg adsorption data

The modes and mechanisms of MG uptake onto MIg can be better understood via isothermal and kinetics data modeling. MG-MIg adsorption data were tested using isotherm equations such as the Langmuir, Freundlich and Temkin (Table 5) and the pseudo first, pseudo second order and intraparticle diffusion model equations were used to test the kinetics data. Chi square was also used for the validation of kinetics data.

Table 5. Mathematical equation for adsorption data analysis.

Isotherms	Equations	Parameters	References
Langmuir	$\frac{C_e}{q_e} = \frac{C_e}{q_{max}} + \frac{1}{q_{max}K_L}$	K_L, R_L, q_{max}	[33]
Freundlich	$R_L = \frac{1}{(1+K_L C_o)}$ $\log q_e = \frac{1}{n}\log C_e + \log K_f$	K_f and n	[34]
Temkin	$q_e = B \ln A + B \ln C_e$ $B = \frac{RT}{b}$	A, B and b	[35]
Kinetics			
Pseudo first order	$\ln(q_e - q_t) = \ln q_e - k_1 t$	q_e and k_1	[36]
Pseudo second order	$\frac{t}{q_t} = \frac{1}{k_2 q_e^2} + \frac{t}{q_e}$	q_e and k_2	[37]
Intraparticle diffusion	$q_t = k_{diff} t^{1/2} + C$	k_{diff} and C	[38]
Kinetics data validation			
Chi square	$\chi^2 = \sum_{i=1}^{n} \frac{(q_{exp} - q_{cal})2}{q_{cal}}$		
Thermodynamics	$\ln K_o = \frac{\Delta S^\circ}{R} - \frac{\Delta H^\circ}{RT}$ ΔS° and ΔH° $\Delta G^\circ = -RT \ln K_o$ ΔG°		

Note: q_e -Quantity of dye adsorbed at equilibrium (mg/g), q_t-Quantity of dye adsorbed at timet (mg/g), C_o-Initial dye concention (mg/L), C_e-Concentration of dye in solution at equilibrium (mg/L), q_{max} Langmuir maximum monolayer adsorption capacity of the adsorbent (mg/g), K_L-Langmuir adsorption constant (L/mg), R_L-Separation factor, K_f-Freundlich constants affecting the adsorption capacity and adsorption intensity, A-Temkin constant (L/g), b-Temkin constant related to the heat of adsorption (J/mol), T-Absolute temperature (K), R-Gas constant (J/mol K), k_1-Pseudo first order rate constants (min⁻¹), k_2-Pseudo second order rate constants (g/mg min⁻¹), K_{diff}-Rate constant for intraparticle diffusion (mgg⁻¹min⁻¹ᐟ²), C-Boundary layer thickness, K_o-Thermodynamic equilibrium constant, ΔH°-Enthalpy change, ΔS° -Entropy change.

Binary and ternary solution treatment

Industries such as textile, plastics, pulp and paper, leather, cosmetics and food industries use dyes with various other chemicals. Hence, their dye effluents come with salts, surfactants and heavy metals amongst others [39, 40]. Binary

92

Orbital: Electron. J. Chem. 12 (2): 87-94, 2020

solution was compost by mixing equal volume of 100 mg/L solution malachite green and rhodamine B (RhB). The ternary solution was compost by mixing equal volume of 100 mg/L solutions of each dye with 60 mg/L solution of Cu^{2+}. The pH of each resulting solutions were obtained. Being a complex mixture of organic compound, each of the solutions were scanned between 500 and 700 nm on a UV-Visible spectrometer (Beckman Coulter Du 730) prior to treatment with 1 mg of MIg. Subsequently, MIg was separated from the treated solutions using centrifuge and separated solution was scanned on the UV-Visible within the aforementioned wavelength. The initial and after treatment concentration of Cu^{2+} were determined using a Pelkin AAnalyte 400 atomic absorption spectrophotometer.

4. Conclusions

MIg was found effective in the removal of MG with optimum pH of 6. However, increased dosage had negligible effect on MG adsorption unto MIg. The Langmuir isotherm model well described the MG-MIg with maximum monolayer adsorption capacity (q_{max}) of 250 mg/g. Adsorption onto non uniform sites also took place in the MG-MIg adsorption system. Pseudo second order kinetics best describe the kinetic data. In the binary and ternary solutions, each dye provided synergy hence aided the removal of the other dye thus treatment of the binary and ternary solutions were effective. The uptake of Cu^{2+} in ternary solution was observed to be very low.

Acknowledgments

References and Notes

[1] Bulgariu, L.; Escudero, L. B.; Bello, O. S.; Iqbal, M.; Nisar, J.; Adegoke, K. A.; Alakhras, F.; Komaros, M.; Anastopoulos, I. *J. Mol. Liq.* **2019**, *276*, 728. [Crosrref]

[2] Kim, D. J.; Jo, W. *Appl. Catal., B* **2019**, *242*, 171. [Crossref]

[3] Hussain, S.; Quinn, L.; Li, J.; Casey, E.; Murphy, C. D. *Int. Biodeterior. Biodegrad.* **2017**, *125*, 142. [Crossref]

[4] Zhou, Z.; Fu, Y.; Qin, Q.; Lu, X.; Shi, X.; Zhao, C.; Xu, G. *J. Chromatogr. A* **2018**, *1560*, 19. [Crossref]

[5] Khera, R. A.; Iqbal, M.; Jabeen, S.; Abbas, M.; Nazir, A.; Nisar, J.; Ghaffar, A.; Shar, G. A.; Tahir, M. A. *Surf. Interfaces* **2019**, *14*, 138. [Crossref]

[6] Banerjee, S.; Mukherjee, S.; LaminKa-ot, A.; Joshi S. R.; Mandal, T.; Halder, G. *J. Adv. Res.* **2016**, *7*, 597. [Crossref]

[7] Rezk, R. A.; Galmed, A. H.; Abdelkreema, M.; Abdel Ghany, N. A.; Harith, M. A. *J. Adv. Res.* **2018**, *14*, 1. [Crossref]

[8] Adekola, F. A.; Ayodele, S. B.; Inyinbor, A. A. *Chem. Data Collect.* **2019**, *19*, 100170. [Crossref]

[9] Zhou, L.; Zhou, H.; Hu, Y.; Yan, S.; Yang, J. *J. Environ. Manage.* **2019**, *234*, 245. [Crossref]

[10] Chaari, I.; Fakhfakh, E.; Medhioub, M.; Jamoussi, F. *J. Mol. Struct.* **2019**, *1179*, 672. [Crossref]

[11] Nabbou, N.; Belhachemi, M.; Boumelik, M.; Merzougui, T.; Lahcene, D.; Harek, Y.; Zorpas, A. A.; Jeguirim, M. *C. R. Chim.* **2018**, *22*, 105. [Crossref]

[12] Liao, C.; Ali, M. B.; Wang, F.; Chu, Y.; Mahmoud, A.; Lei, W.; Boukherroub, R.; Xia, M. *J. Environ. Sci.* **2019**. [Crossref]

[13] Castillo, X.; Pizarro, J.; Ortiz, C.; Cid, H.; Flores, M.; Canck, E. D.; Voort, P. V. D. *Microporous Mesoporous Mater.* **2018**, *272*, 184. [Crossref]

[14] Tomasz, K.; Anna, K.; Ryszard, C. *Microchem. J.* **2019**, *145*, 1011. [Crossref]

[15] Ziane, S.; Bessaha, F.; Marouf-Khelifa, K.; Khelifa, A.; *J. Mol. Liq.* **2018**, *249*, 1245. [Crossref]

[16] Bentahar, S.; Dbik, A.; El Khomri, M.; El Messaoudi, N.; Lacherai, A. *J. Environ. Chem. Eng.* **2017**, *5*, 5921. [Crossref]

[17] Roy, A.; Bhattacharya, J. *Sep. Purif. Technol.* **2013**, *115*, 172. [Crossef]

[18] Inyinbor, A. A.; Adekola, F. A.; Olatunji, G. A. *S. Afr. J. Chem.* **2015**, *68*, 115. [Crossref]

[19] Gautam, D.; Kumari, S.; Ram, B.; Chauhan, G. S.; Chauhan, K. *J. Environ. Chem. Eng.* **2018**, *6*, 3889. [Crossref]

[20] Lara-Vásquez, E. J.; Solache-Ríos, M.; Gutiérrez-Segura, E. *J. Environ. Chem. Eng.* **2016**, *4*, 1594. [Crossref]

[21] Bouaziz, F.; Koubaa, M.; Kallel, F.; Ghorbel, R. E.; Chaabouni, S. E. *Int. J. Biol. Macromol.* **2017**, *105*, 56. [Crossref]

[22] Sartape, A. S.; Mandhare, A. M.; Jadhav, V. V.; Raut, P. D.; Anuse, M. A.; Kolekar, S. S. *Arabian J. Chem.* **2017**, *10*, S3229. [Crossref]

[23] Gan, L.; Zhou, F.; Owens, G.; Chen, Z. *Colloids Surf., B* **2018**, *172*, 526. [Crossref]

[24] Rangabhashiyam, S.; Balasubramanian, P. *Bioresource Technology Reports* **2018**, *3*, 75.

[25] Altintig, E.; Onaran, M.; Sarı, A.; Altundag, H.; Tuzen, M. *Mater. Chem. Phys.* **2018**, *220*, 313. [Crossref]

93

Orbital: Electron. J. Chem. 12 (2): 87-94, 2020

[26] Zaidi, N.; Lim, L. B. L.; Usman, A. *Environmental Technology & Innovation* **2019**, *13*, 211. [Crossref]

[27] Mashkoor, F.; Nasar, A. *J. Mol. Liq.* **2019**, *274*, 315. [Crossref]

[28] Murthy, T. P. K.; Gowrishankar, B. S.; Prabha, M. N. C.; Kruthi, M.; Krishna, R. H. *Microchem. J.* **2019**, *146*, 192. [Crossref]

[29] Inyinbor, A. A.; Adekola, F. A.; Dada, A. O.; Oluyori, A. P.; Olatunji, G. A.; Fanawopo, O. F.; Oreofe, T. A. *Environmental Technology & Innovation* **2019**, 13, 37. [Crossref]

[30] Huang, Y.; Zheng, X.; Feng, S.; Guo, Z.; Liang, S. *Colloids Surf., A* **2016**, *489*, 154. [Crossref]

[31] Inyinbor, A. A.; Adekola, F. A.; Olatunji, G. A. *Appl. Water Sci.* **2017**, *7*, 3257. [Crossref]

[32] Negara, D. N. K. P.; Nindhia, T. G. T.; Surata, I. W.; Fadjar Hidajat, F.; Sucipta, M. *Surf. Interfaces* **2019**, *16*, 22. [Crossref]

[33] Langmuir, I. *J. Am. Chem. Soc.* **1916**, *38*, 2221. [Crossref]

[34] Freundlich, H. M. F. *Z. Phys. Chem.* **1906**, *57*, 385.

[35] Temkin, M. I.; Pyzhev, V. *Acta Physiochimica USSR* **1940**, *12*, 327.

[36] Lagergren, S.; Svenska, B. K. *R. Swed. Acad. Sci. Doc, Band* **1898**, *24*, 1.

[37] Ho, Y. S.; McKay, G. *Proc. Biochem.* **1999**, *34*, 451. [Crossref]

[38] Weber, W. J.; Morris, J. C. *J. Sanity Eng. Div. Am. Soc. Civil Eng.* **1963**, *89*, 31

[39] GilPavas, E.; Dobrosz-Gómez, I.; Gómez-García, M. Á. *Journal of Water Process Engineering* **2018**, 22, 73. [Crossref]

[40] Costa, A. F. S.; Albuquerque, C. D. C.; Salgueiro, A. A.; Sarubbo, L. A. *Process Saf. Environ. Prot.* **2018**, *118*, 203. [Crossref]

94

Orbital: Electron. J. Chem. 12 (2): 87-94, 2020